

# A simple model for the evolution of super-massive black holes and the quasar population

Asim Mahmood<sup>1\*</sup>, Julien E. G. Devriendt<sup>1,2</sup> and Joseph Silk<sup>1</sup>

<sup>1</sup>*Department of Astrophysics, University of Oxford, Keble Road, Oxford, OX1 3RH, U.K*

<sup>2</sup>*Observatoire Astronomique de Lyon, 9 Avenue Charles André, 69561 Saint-Genis Laval cedex, France*

Received ...; accepted ...

## ABSTRACT

An empirically motivated model is presented for accretion-dominated growth of the super massive black holes (SMBH) in galaxies, and the implications are studied for the evolution of the quasar population in the universe. We investigate the core aspects of the quasar population, including space density evolution, evolution of the characteristic luminosity, plausible minimum masses of quasars, the mass function of SMBH and their formation epoch distribution. Our model suggests that the characteristic luminosity in the quasar luminosity function arises primarily as a consequence of a characteristic mass scale above which there is a systematic separation between the black hole and the halo merging rates. At lower mass scales, black hole merging closely tracks the merging of dark haloes. When combined with a declining efficiency of black hole formation with redshift, the model can reproduce the quasar luminosity function over a wide range of redshifts. The observed space density evolution of quasars is well described by formation rates of SMBH above  $\sim 10^8 M_\odot$ . The inferred mass density of SMBH agrees with that found independently from estimates of the SMBH mass function derived empirically from the quasar luminosity function.

**Key words:** cosmology: dark matter – galaxies: formation – galaxies: active – quasars: general

## 1 INTRODUCTION

Super massive black holes consisting of at least tens of millions of solar masses are now believed to be lurking in the nuclei of most galaxies. These dark objects are also the central engines of the most powerful sources of light in the universe: the quasars. Discerning the evolution history of SMBHs and quasars is a fundamental challenge for the theories of structure formation in the universe. Quasars and other forms of Active Galactic Nuclei (AGN) are thought to be powered by accretion on to the SMBHs. By virtue of their enormous brightness these objects are now observable up to sufficiently high redshifts, corresponding to the dawn of the era of galaxy and star formation in the universe. In the context of hierarchical structure formation, it is believed that mergers of galaxies play a crucial role in igniting the quasars. The merger induced gravitational instabilities funnel a huge amount of gas to the galactic cores. As a fraction of the kinetic energy of this gas is released in the form of electromagnetic radiation, luminosities close to the Eddington luminosity ( $\sim 10^{46}$  erg s<sup>-1</sup> for a typical  $\sim 10^8 M_\odot$  SMBH masses) are produced.

Nuclear black holes probably trace the merger of their host galaxies and coalesce during mergers. If one envisages a simple scenario where a dark matter halo harbours a single galaxy and halo merging leads to galaxy merging along with their SMBHs, a coalescence dominated growth naturally leads to a linear relation between the black hole and the host halo masses (see e.g. Haehnelt, Natarajan & Rees 1998, hereafter HNR98). The observed correlation between the black hole masses and the bulge velocity dispersion ( $M_{BH} - \sigma$  relation) of galaxies (Ferrarese & Merritt 2000), however, suggests that the accreted component of mass far supersedes the coalesced one. The observed scaling is concomitant with a scenario where the energy feedback from the black hole plays a crucial role in regulating the amount of matter accreted on to it (Silk & Rees 1998). During the accretion process the mass of the SMBH builds up over some characteristic time-scale. The ratio of this characteristic time-scale to the Hubble time determines the duty cycle of a quasar. Accretion shuts down when the black hole is so massive that its energy feedback exceeds the binding energy of its fuel reservoir. Indeed, as pointed out by HNR98 and Wyithe & Loeb (2003), the observed scaling can be retrieved if the black hole were to supply the gas with an energy equal to its binding energy over the dynamical time of galaxies. These intricately

\* E-mail: mahmood@astro.ox.ac.uk

woven, yet neat set of ideas sketch an outline for simple models of quasar and SMBH evolution.

Several analytic and semi-analytic models based on mergers of dark haloes have been proposed to explain the high redshift evolution of quasar luminosity functions (see for e.g. Haehnelt & Rees 1993, hereafter HR93; HNR98; Haiman & Loeb 1998; Kauffmann & Haehnelt 2000, hereafter KH00; Cavaliere & Vittorini 2000, hereafter CV00; Hosokawa 2002; Wyithe & Loeb 2003, hereafter WL03; Hatziminaoglou et al. 2003). Simplified analytic models assume that all the cold baryons in a halo are locked in a single galaxy and galaxy mergers trace the halo mergers. More realistically, the progenitor galaxies in a newly formed halo sink towards the centre over a dynamical friction time-scale (Binney & Tremaine 1989; Lacey & Cole 1993) and merge to form a new baryonic core. However, as the dynamical friction time-scale is generally much shorter than the Hubble time, the approximation that these mergers are instantaneous, works rather well. Galactic mergers are assumed to ignite an AGN lasting for a characteristic time  $t_{qso}$ . The resulting luminosities are estimated as Eddington luminosities corresponding to central black hole masses, which in turn are determined through their correlation with the circular velocities of the newly formed haloes.

The uncertainty in the mass of cold gas available for accretion poses a key difficulty for the models. There are two central aspects of this uncertainty: the first is to ascertain how much cold gas is available in galaxies of a given mass at a given epoch (Kauffmann & Haehnelt 2000) and the second is to understand how effectively this gas is transported via the galaxy mergers to become available for accretion by the forming SMBH (Cavaliere & Vittorini 2000).

The predictions of these models can be tested against the backdrop of a fairly well constrained observational data set. The most striking aspect of this data is that the quasar population peaks at  $z \sim 2.5$  and exhibits a steep decline towards lower redshifts (Schmidt, Schneider & Gunn 1995; Warren, Hewett & Osmer 1994; Shaver et al. 1996; Boyle et al. 2000). At redshifts higher than  $\sim 2.5$  the number count appears to decline again, however, the observations at these redshift could be marred by obscuration and extinction effects. Simple analytical models mentioned above can well explain the high redshift observed luminosity functions ( $z \gtrsim 2$ ). They, however, systematically fail at lower redshifts ( $z \lesssim 2$ ) and this epoch in the history of the universe is somewhat opaque in our understanding of the evolution of quasars. Even though the works of CV00, HR93 and KH00 shed important light in this regard, no comprehensive scheme is yet available to systematically quantify the various aspects of quasar evolution at  $z \lesssim 2$ .

The present work is primarily motivated by the low redshift anomaly between observations and theoretical predictions. To bridge this gap we introduce a toy model centred around two main ideas: the first pertains to the effect of declining black formation efficiency at low redshifts and the second involves a declining black hole formation rate in haloes above some characteristic mass  $M_*$ . The first idea is derived from a model investigated in Haehnelt & Rees (1993) where it is argued that the conditions for SMBH formation are more favourable at higher redshifts as compared to low redshifts. The second idea is based on the existence of a break luminosity in the empirical quasar lu-

minosity functions. We attribute this break luminosity to a systematic decoupling between halo and galaxy merger rates in haloes above a characteristic mass along the line suggested by CV00 that galaxy merging becomes rarer in sufficiently massive haloes, where individual galaxies retain their properties. Furthermore, in a similar context, Haiman, Ciotti & Ostriker (2003) have argued that a decrease in the quasar luminosity density towards low redshifts arises due to a decline in the formation rates of spheroids. Here we propose a characteristic mass scale  $M_*$  for haloes which marks a drop in the formation rates of black holes and thus possibly spheroids as well. As the low redshift universe is an era of group assemblage, our value of  $M_*$  which corresponds to a group mass scale seems natural to explain the steep decline observed in the quasar luminosity density at low  $z$ .

Our model entails a phenomenological treatment of the ideas described above. Notwithstanding the crudeness of the approach, it yields interesting results for the the quasar luminosity functions and their evolving number density, broadly consistent with the observations. It also provides a simple explanation for the evolution of the characteristic luminosity of quasars. Furthermore, the minimum SMBH masses for quasars suggested by the model (by comparison with the observed space density evolution of quasars) are  $\gtrsim 10^8 M_\odot$ , which is consistent with the original estimates of Soltan (1982). Finally the model can be linked quite simply with the evolution of cold gas masses in galaxies and star formation rates in the universe and thus yields estimates of the contributions to the ionising background at high redshifts, due to star formation and quasar activity.

The structure of the paper is as follows: in section 2 we review some important aspects of analytical modelling of hierarchical structure formation which provides the essential tools for our model; section 3 discusses the relation between the black hole masses and their host haloes in a scenario with a declining efficiency of SMBH formation with redshift. Section 4 extends the argument of major mergers of haloes to compute the SMBH formation rates and the luminosity functions of the ensuing quasars. In section 5 we compare the SMBH formation rates from our model against those inferred from the empirical double power-law fit to the quasar luminosity functions. In section 6 we estimate the mass functions of SMBH and the comoving cosmological mass density in the SMBH at various redshifts. Section 7 describes how to obtain simple estimates of the cold gas density and star formation rate density in the universe; section 8 extrapolates these star formation rates to high redshift to compute the ionising background. These are then compared with a similar extrapolation to high redshifts, of the quasar luminosity density. We summarise and discuss our results in section 9.

## 2 ELEMENTS FROM EXTENDED PRESS-SCHECHESTER THEORY

Our approach largely takes advantage of the extended Press-Schechter (EPS) formalism which provides essential tools for computing the merger probabilities and rates of bound objects (Bond et al. 1991; Bower 1991; Lacey & Cole 1993, hereafter LC93). In this scenario the initial density fluctuations in the universe are assumed to be Gaussian in nature.

The growth of these fluctuations proceeds linearly initially and is analysed through the linearised ideal fluid equations (e.g. Silk & Bouwens 2001). The fluctuations subsequently turn non-linear and eventually collapse to form bound objects as the density reaches a critical threshold. A comparison of EPS results with the results of N-body simulations as given in Lacey & Cole (1994), demonstrates that the prescription works rather well.

The linear growth of fluctuations is described through the linear growth factor  $D(t)$ . For a critical cosmology this factor is simply equal to the scale factor  $a$  for that epoch. For the  $\Lambda$ CDM cosmology used in this paper ( $\Omega_m^0 = 0.3$ ,  $\Omega_\Lambda^0 = 0.7$ ,  $\Omega_b^0 = 0.02/h^2$ ,  $\sigma_8 = 0.9$ ,  $h = 0.7$ ), we compute it as given in Navarro, Frenk & White (1997). The mass  $M$  of an inhomogeneity is represented through a sharp  $k$ -space filter which is used to smooth the matter density field at this mass scale. As suggested in LC93,  $M$  can be related to  $k_s$  through a qualitative mapping  $M = 6\pi^2\rho_0 k_s^{-3}$ . Here  $\rho_0$  is the mean background density of matter in the universe. Using the dark matter power-spectrum  $P(k)$  parametrized as in Efstathiou, Bond & White (1992), the variance for mass scale  $M$  can then be simply calculated as

$$\sigma^2(M) = \int_0^{k_s} P(k) 4\pi k^2 dk. \quad (1)$$

The mass function of haloes is now written in terms of  $\sigma^2(M)$  as

$$N_{PS}(M, t) = \sqrt{\frac{2}{\pi}} \frac{\bar{\rho}_0}{M} \frac{\omega}{D(t)} \left| \frac{1}{\sigma^2} \frac{d\sigma}{dM} \right| \exp \left[ -\frac{1}{2} \frac{\omega^2}{D^2(t)\sigma^2} \right], \quad (2)$$

where  $\omega$  is the critical density for collapse.

The formation rates, major merger rates and survival probabilities have been discussed by several authors (e.g. Sasaki 1994; Kitayama & Suto 1996, hereafter KS96). In this context, the excursion set approach of Bond et al. (1991) (also LC93) yields two important conditional probabilities. The first is the conditional probability that a halo of given mass  $M_2$  at time  $t_2$ , had a progenitor of mass  $M_1$  at earlier time  $t_1$ . This is given as

$$P_1(S_1, \omega_1 | S_2, \omega_2) dS_1 = \frac{1}{\sqrt{2\pi}} \frac{(\omega_1 - \omega_2)}{(S_1 - S_2)^{3/2}} \times \exp \left[ -\frac{(\omega_1 - \omega_2)^2}{2(S_1 - S_2)} \right] dS_1, \quad (3)$$

where  $\omega_1$  is the critical density at time  $t_1$  and  $\omega_2$  at time  $t_2$ . Also,  $S_1$  is the variance corresponding to mass  $M_1$  and  $S_2$  is the variance corresponding to  $M_2$ . The relation between the critical density  $\omega(t)$  at any time  $t$  is given as  $\omega(t) = \omega_0/D(t)$ , where  $\omega_0$  is the present day critical density ( $\sim 1.686$  for a  $\Lambda$ CDM cosmology).

The second is the probability that a halo of mass  $M_1$  at time  $t_1$ , will result in a larger halo of mass  $M_2$  at later time  $t_2$  can be written as

$$P_2(S_2, \omega_2 | S_1, \omega_1) dS_2 = \frac{1}{\sqrt{2\pi}} \frac{\omega_2(\omega_1 - \omega_2)}{\omega_1} \left[ \frac{S_1}{S_2(S_1 - S_2)} \right]^{3/2} \times \exp \left[ -\frac{(S_2\omega_1 - S_1\omega_2)^2}{2S_1S_2(S_1 - S_2)} \right] dS_2. \quad (4)$$

Through appropriate transformations the conditional probabilities can also be written in terms of halo masses.

## 2.1 Merger rates, survival probabilities and formation epoch distributions

The EPS formalism lacks a self sufficient way to compute the formation rates of haloes. This is because effectively all haloes at any epoch are continuously accreting mass and in this sense are newly created. There is no clear distinction between the objects accreting less mass and the objects which accrete substantial mass. For computing the major merger rates, therefore, a criterion has to be introduced by hand. One has to assume that if none of the progenitors of a newly formed object had mass greater than half (or some other fraction) of the object mass, the event is a major merger. Alternatively Sasaki (1994) proposed to derive the formation rates by assuming that the destruction probability of objects (i.e. the probability that they get incorporated into higher mass objects) has no characteristic mass scale. This rate is then simply the positive term in the time derivative of the PS mass function. In Sasaki's prescription the survival probability of haloes from one redshift to another is simply the ratio of the growth factors at these redshift. The product of formation rate and the survival probability defines the formation epoch distribution. Interestingly for a critical cosmology, Sasaki's formation epoch distribution can be integrated analytically over all redshifts to yield the exact mass function of haloes.

In the present work we compute the major merger rates based on the prescriptions described in LC93 and KS96. The probability that a given halo of mass  $M_2$  at time  $t_2$  had, at some earlier time  $t_1$ , a progenitor with mass below some threshold mass  $M_c (< M_2)$  is computed by integrating equation 3 over  $S_1$  from  $S(M_c)$  to  $\infty$ . If the difference between the times  $t_1$  and  $t_2$  is substantial, then  $M_1$  can reach the value  $M_2$  through either a single merger occurring anytime between  $t_1$  and  $t_2$  or it can do so through more than one merger/accretion episodes between the two times. However, if the difference between the two times is very small then the entire change in mass ( $\Delta M = M_2 - M_1$ ) can be treated as arising from a single merging event. Letting  $\Delta\omega = \omega_1 - \omega_2$  we thus write

$$P(M_1 < M_c, t_1 | M_2, t_2) = \int_0^{M_c} P_1 dM_1 \quad (5) \\ = \text{erf} \left[ \frac{\Delta\omega}{\sqrt{2(S_c - S_2)}} \right],$$

where  $S_c$  is the variance corresponding to mass  $M_c$ . For small  $\Delta\omega$  taking the series expansion in equation 5 up to first order only, we compute the major merger rates of dark haloes as

$$R_{MM}(M, t) = \sqrt{\frac{2}{\pi}} \frac{1}{\sqrt{S(M/2) - S(M)}} \times \left| \frac{d\omega}{dt} \right| N_{PS}(M, t), \quad (6)$$

where we have chosen  $M_c = M/2$ . Note that when  $S_c$  tends to  $S$ , the right hand side of equation 5 tends to one, if  $\Delta\omega$  is small but finite. This implies that at any given epoch, all the existing objects continuously accrete mass.

As pointed out in LC93, when the halo mass for a trajectory falls to a smaller value at an earlier time, it only means that *one* of the parent haloes had this smaller mass. As a result, it is always possible that the largest coeval progenitor already has more than half the mass of the final halo

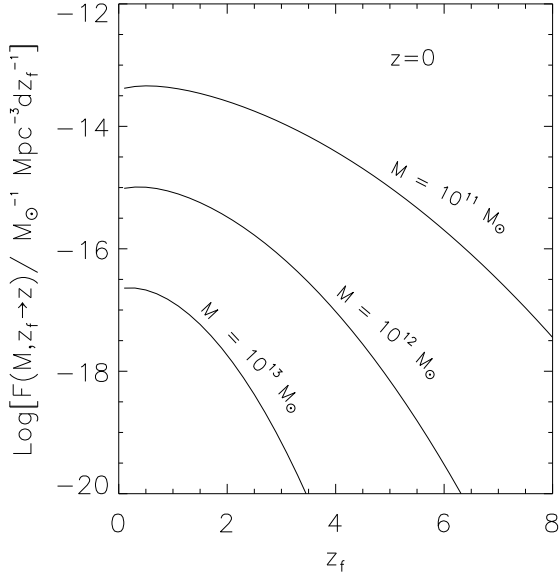


**Figure 1.** The formation epoch distribution of DM haloes of different masses as given by equation 8.

at this epoch. Such an event cannot be characterised as a major merger as we define it. The approach of KS does not account for this possibility. Although this marginally alters the rates for the range of halo masses we are concerned with, it is nevertheless interesting to see how one can systematically account for this possibility and therefore, we propose a solution to this problem in appendix A.

Equation 4 can be used to calculate the survival probabilities as discussed in LC93 and KS96. These are based on the assumption that an object retains its identity up to the time it doubles its mass. The probability that a halo of mass  $M$  at present time  $t_1$ , will not undergo such a merger/accretion, before time  $t_2$ , which would result in its final mass being greater than  $2M$ , is given as

$$P_{surv}(M, t_1, t_2) = \int_M^{2M} P_2(M_2, t_2 | M, t_1) dM_2. \quad (7)$$

As discussed previously, the survival probability of haloes multiplied with their merger rates, yields their formation epoch distribution. This distribution tells us that in a given population of mass  $M$  objects at time  $t$ , what fraction were formed at an earlier time  $t_f$  and have retained their identity since then. Thus the formation epoch distribution in terms of formation time  $t_f$  can be written as

$$F(M, t_f \rightarrow t) dM dt_f = R_{MM}(M, t_f) \times P_{surv}(M, t_f \rightarrow t) \times dM dt_f. \quad (8)$$

We show in Fig 1 the formation epoch distribution of haloes of different masses as a function of redshift, and in Fig 2 the formation rates of objects with masses above  $10^{11}$ ,  $10^{12}$  and  $10^{13} M_\odot$  respectively. It can be seen from Fig 2 that merger rates of haloes alone do not produce a significant evolution in the number density at low  $z$ , and therefore a naive model directly linking quasar triggering to merger rates of haloes would fail to match the steep decline which is observed in

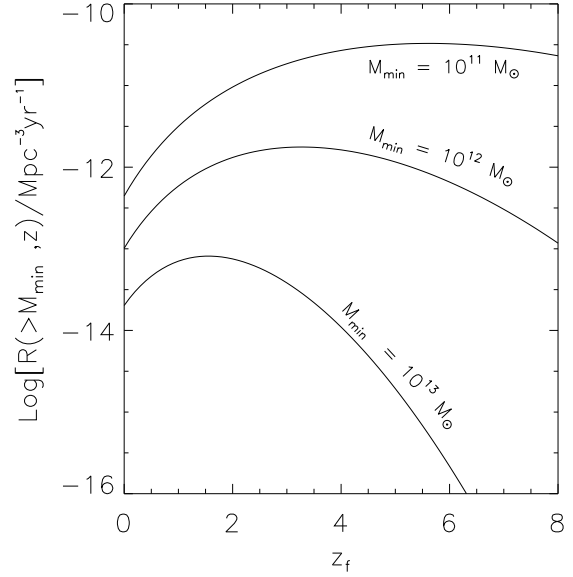


**Figure 2.** The evolution of cumulative formation rates of dark matter haloes with masses above  $M_{min}$ . These rates (particularly for  $M_{min} = 10^{12} M_\odot$ , the typical quasar host halo mass) do not produce as steep a decline at low redshifts as that measured for quasar number counts.

their number density. Hence, we subsequently discuss the additional inputs that need to be incorporated into the model in order to reproduce the observed evolution of the quasar population.

## 2.2 Halo circular velocities

For a nearly isothermal halo, the mapping between the halo circular velocity and its mass can be obtained using the relations given in Somerville & Primack (1999)

$$v_c^2 = \frac{GM}{r_{vir}(z)} - \frac{\Omega_\Lambda}{3} H_0^2 r_{vir}^2(z), \quad (9)$$

where  $z$  is the collapse redshift and  $r_{vir}$  is the virial radius.  $r_{vir}$  can be computed by noting that  $M = 4\pi/3 r_{vir}^3(z) \rho_{vir}(z)$  where the virial density  $\rho_{vir}(z)$  is given as

$$\rho_{vir}(z) = \Delta_c(z) \rho_c^0 (1+z)^3 \frac{\Omega_0}{\Omega(z)}. \quad (10)$$

Here,  $\Omega_0$  and  $\Omega(z)$  are the matter densities of the present day and redshift  $z$  universe respectively;  $\rho_c^0 = 2.8 \times 10^{11} h^2 M_\odot \text{Mpc}^{-3}$  is the present critical density of the universe and a fitting expression for  $\Delta_c(z)$  is given as  $\Delta_c(z) = 18\pi^2 + 82x - 38x^2$ , where  $x = \Omega_m(z) - 1$  (Bryan & Norman 1998). Thus the expression for virial radius in terms of formation redshift  $z$  and halo mass  $M$  is given as

$$r_{vir} = 2.14 \times 10^{-5} M^{1/3} \left[ \frac{\Omega_m^0}{\Omega_m(z)} \frac{\Delta_c(z)}{18\pi^2} \right]^{-1/3} (1+z)^{-1} \text{Mpc}. \quad (11)$$

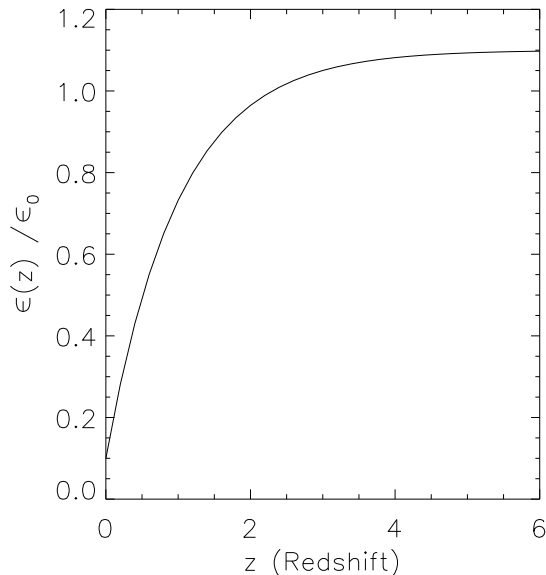


**Figure 3.** Phenomenological redshift evolution of the formation efficiency of black holes (see text for the exact function). The characteristic redshift of decline is  $z_* = 1$ . A steep decline is obtained around  $z = 0$  where values become as low as ten percent of the maximum value.

These relations together enable us to write the halo circular velocity as

$$v_c = 1.38 \times 10^{-2} M^{1/3} \left[ \frac{\Omega_m^0}{\Omega_m(z)} \frac{\Delta_c(z)}{18\pi^2} \right]^{1/6} (1+z)^{1/2} \text{ kms}^{-1}. \quad (12)$$

### 3 SUPER MASSIVE BLACK HOLE MASSES

In a self-regulated growth of SMBH masses, the correlation between the galaxy circular velocities ( $v_c$ ) and SMBH masses ( $M_{BH}$ ) is written as (Silk & Rees 1998)

$$M_{BH} \propto v_c^5, \quad (13)$$

where the constant of proportionality depends on the fraction of cold gas  $f_{cold}$  available for accretion by the coalesced seed black hole and weakly on the presence of an accretion disc (HNR98; Burkert & Silk 2001). Such a scaling is corroborated by the investigations of Ferrarese & Merritt (2000) and Gebhardt et al. (2000).

Incorporating  $f_{cold}$  in an analytic model is not simple. Firstly, we do not know how much cold gas exists in haloes of different masses at different epochs and secondly, even if we knew the mass of cold gas, it is impossible to analytically compute the contributions coming from different mass progenitors during a merger. For the sake of simplicity, therefore, we get around this problem by adopting an empirically motivated decline in black hole formation efficiency with redshift. This can be attributed to a general decline in the amount of cold gas in the galaxies at low redshifts. Such an approach has been considered previously, for example, by Haehnelt & Rees (1993).

We model the declining formation efficiency of SMBH masses through a function  $\epsilon(z)$  such that  $M_{BH} = \epsilon(z) v_c^5$  and consider a phenomenological form of  $\epsilon(z)$  as

$$\epsilon(z) = \epsilon_0 \times \left[ c - \exp\left(-\frac{z}{z_*}\right) \right]. \quad (14)$$

Here  $\epsilon_0$  and  $c$  are constants and  $z_*$  is a characteristic redshift. We choose a value  $z_* \approx 1$  based on the observed peak in the star formation rate (SFR) density in the universe at redshifts between 1 and 2 (see e.g. Ascasibar et al. 2002; Silk & Rees 1998). This is because a peak in the SFR density is a general indicator of a gas rich environment in galaxies. It is, however, still a matter of debate whether SFR density peaks at  $z \sim 1-2$  or reaches a broad maximum there. To obtain a steep decline we choose  $c = 1.1$  such that the minimum value of  $\epsilon(z)$  is roughly 10 percent of the maximum value  $1.1 \times \epsilon_0$ . This latter is chosen to match the observed  $M_{BH} - \sigma$  correlation (Ferrarese 2002)

$$M_{BH} = 1.66 \times 10^8 \left( \frac{\sigma}{200 \text{ km s}^{-1}} \right)^\alpha M_\odot, \quad (15)$$

where we adopt  $\alpha = 5$  consistent with a feedback regulated growth of SMBH masses. This is slightly different from the value  $\alpha = 4.58 \pm 0.52$  inferred from SMBH mass measurements, the difference possibly having its origin in the observed non-linearity of  $v_c - \sigma$  relation (Ferrarese 2002; WL03). For simplicity, we consider the linearly fitted relation for ellipticals  $\sigma \approx 0.65 v_c$  to obtain  $\epsilon_0 = 6 \times 10^{-5}$  (such that  $M_{BH} \sim \epsilon_0 v_c^5$  at high redshifts).

Figure 3 shows a plot of efficiency versus the formation redshift, i.e. how equation 14 behaves. We can now write the black hole masses in terms of formation redshift  $z$  and halo masses  $M$  as

$$M_{BH} = \epsilon(z) \times 5 \times 10^{-10} \left( \frac{M}{M_\odot} \right)^{5/3} \times \left[ \frac{\Omega_m^0}{\Omega_m(z)} \frac{\Delta_c(z)}{18\pi^2} \right]^{5/6} (1+z)^{5/2} M_\odot. \quad (16)$$

### 4 FORMATION RATES OF SMBH AND QUASAR LUMINOSITY FUNCTIONS

We now use the  $M_{BH} - M_{halo}$  mapping (equation 16) to transform the halo major merger rates into the black hole formation rates in terms of the formation redshift  $z$  as

$$R_{BH}^1(M_{BH}, z) = R_{MM}[M_{halo}(M_{BH}, z), z] \frac{dM}{dM_{BH}}(M_{BH}, z). \quad (17)$$

The superscript 1 in  $R_{BH}^1$  is to differentiate it from a modified rate  $R_{BH}$ , which takes into account a decline in black hole formation rates in haloes above a characteristic mass  $M_*$ . This is achieved through a phenomenological function  $F_\mu(M_{halo})$  such that

$$R_{BH}(M_{BH}, z) = R_{BH}^1(M_{BH}, z) \times F_\mu[M_{halo}(M_{BH}, z)]. \quad (18)$$

For the form of  $F_\mu(M_{halo})$ , we found that a simple exponential function  $\exp(-M/M_*)$ , with a cutoff at  $M_*$  is too steep to be consistent with the observed luminosity functions. We therefore adopt a function with a following behaviour:  $F(M) \rightarrow 1$  for  $M \ll M_*$  and  $F(M) \rightarrow (M_*/M)^\mu$  for  $M \gg M_*$ , where  $\mu$  is a positive number. Instead of a

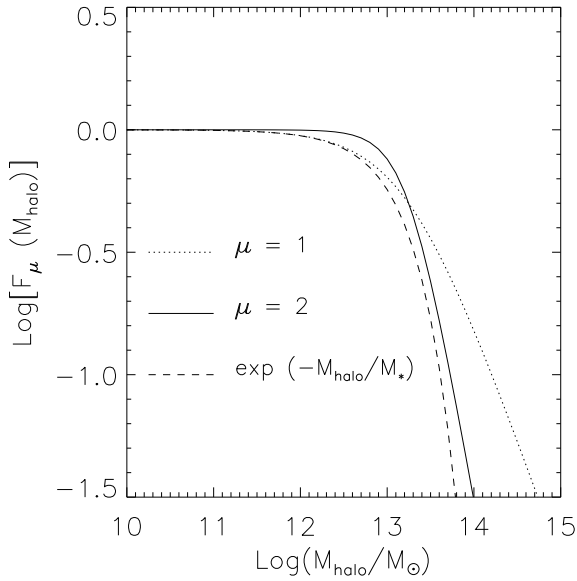


**Figure 4.** This figure shows the second of our two phenomenological functions. We use this function to introduce a drop in the formation rates of black hole in haloes above the characteristic mass scale  $M_*$ , the value of which has been set by comparison with the quasar luminosity function (figure 21) to about  $M_* = 10^{13.25} M_\odot$ . The redshift evolution of the luminosity corresponding to this characteristic mass is plotted against the empirical characteristic luminosity of the double power law fit, in fig 7.

sharp exponential cut-off, such a function has softer ‘power-law’ drop at the high mass end:

$$F_\mu(M) = \frac{1}{1 + (M/M_*)^\mu}. \quad (19)$$

$F_\mu(M)$  for values of  $\mu = 1$  and  $\mu = 2$  is plotted in figure 4 along with the exponential function  $F(M) = \exp(-M/M_*)$ .

It is important to mention at this point that in massive haloes ( $M > M_*$ ), rarer galaxy mergers could possibly alter the  $M_{BH} - M_{halo}$  mapping. Furthermore, the AGN could enter the sub-Eddington regime due to lack of gas mass transported through rare galaxy mergers. However, to keep our model simple we assume that even for ineffective galaxy mergers, the  $M_{BH} - M_{halo}$  scaling is as given in equation 16. If a merger-ignited black hole shines at the Eddington luminosity  $L_{bol}/L_{Edd} = 1$ , we can write the B-band luminosities of AGNs as

$$L_B = f_B \times 1.3 \times 10^{39} \left[ \frac{M_{BH}}{10^8 M_\odot} \right] \text{ J s}^{-1}, \quad (20)$$

where  $f_B$  is the fraction of bolometric luminosity emitted in the B-band. Realistically, as the accretion proceeds, the black hole mass builds up over the characteristic accretion time. This process is accompanied by a parallel increase in the quasar luminosity which determines its light curve. However, a simplification is possible if one considers that the black hole mass instantaneously increases to post merger values given by equation 16. The black hole then shines at the Eddington luminosity, corresponding to this new mass, over characteristic time-scale  $t_{qso}$  which lies in the range  $t_{qso}/t_{Hubble} \sim 10^{-2}$  to  $10^{-3}$ . Thus using the  $L_B - M_{BH}$

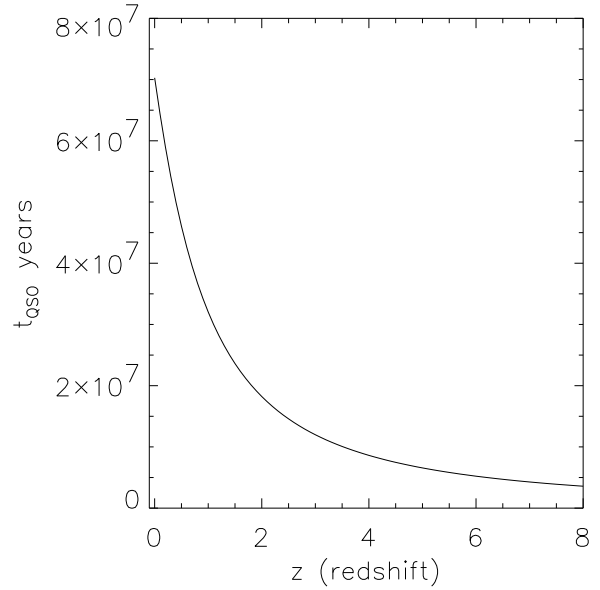


**Figure 5.** The model lifetime of quasars given as  $t_{qso} = k t_{dyn}$ , where  $t_{dyn}$  is the halo dynamical time and the constant of proportionality is about  $k \approx 0.035$  (e.g. WL03)

mapping and the fact that  $t_{qso} \ll t_{Hubble}$  we can simply write the quasar luminosity function as

$$\Phi(L_B, z) \simeq t_{qso} \times R_{BH}[M_{BH}(L_B), z] \times \frac{dM_{BH}}{dL_B}(L_B, z). \quad (21)$$

The quasar lifetime,  $t_{qso}$  is not a very well constrained quantity. Two relevant time-scales for quasars are the Salpeter (or e-folding) time-scale and the dynamical time-scale of galaxies. The Salpeter time-scale is given by  $t_{Sal} = 4 \times 10^7 (\epsilon_{rad}/0.1)$  where  $\epsilon_{rad}$  is the radiative efficiency of black holes defined through the relation  $L_{bol} = \epsilon_{rad} \dot{M} c^2$ ,  $c$  is the speed of light and  $\dot{M}$  is the accretion rate of matter on to the black hole. On the other hand it has been noted, for example, in HNR98 and WL03, that the observed  $M_{BH} - v_c$  relation naturally arises if the black hole injects the gas with an energy equal to its binding energy, over a local dynamical time-scale of the galaxy. In this respect, the local dynamical time of a galaxy is also a natural time-scale. In the present model, following WL03, we adopt a quasar lifetime proportional to the local dynamical time of galaxies in newly formed haloes. The local dynamical time of galaxies being themselves proportional to the halo dynamical time, we get  $t_{qso} \propto t_{dyn}$ , where  $t_{dyn}$  is the halo dynamical time and so we write

$$t_{qso} = k \times 1.5 \times 10^9 \left[ \frac{\Omega_m^0}{\Omega_m(z)} \frac{\Delta_c(z)}{18\pi^2} \right]^{-1/2} (1+z)^{-3/2} \text{ yr}, \quad (22)$$

where the constant of proportionality is  $k \sim 0.035$  (e.g. WL03).

In figure 6 we plot the luminosity functions as given by equation 21 (solid curves). The parameters are  $\mu = 2$ ,  $M_* = 10^{13.25} M_\odot$  and  $f_B = 0.06$ . The short-dashed curve is the double power law fit as given in Pei (1995). We transform the data and the double power-law fit to a  $\Lambda$  cosmology by

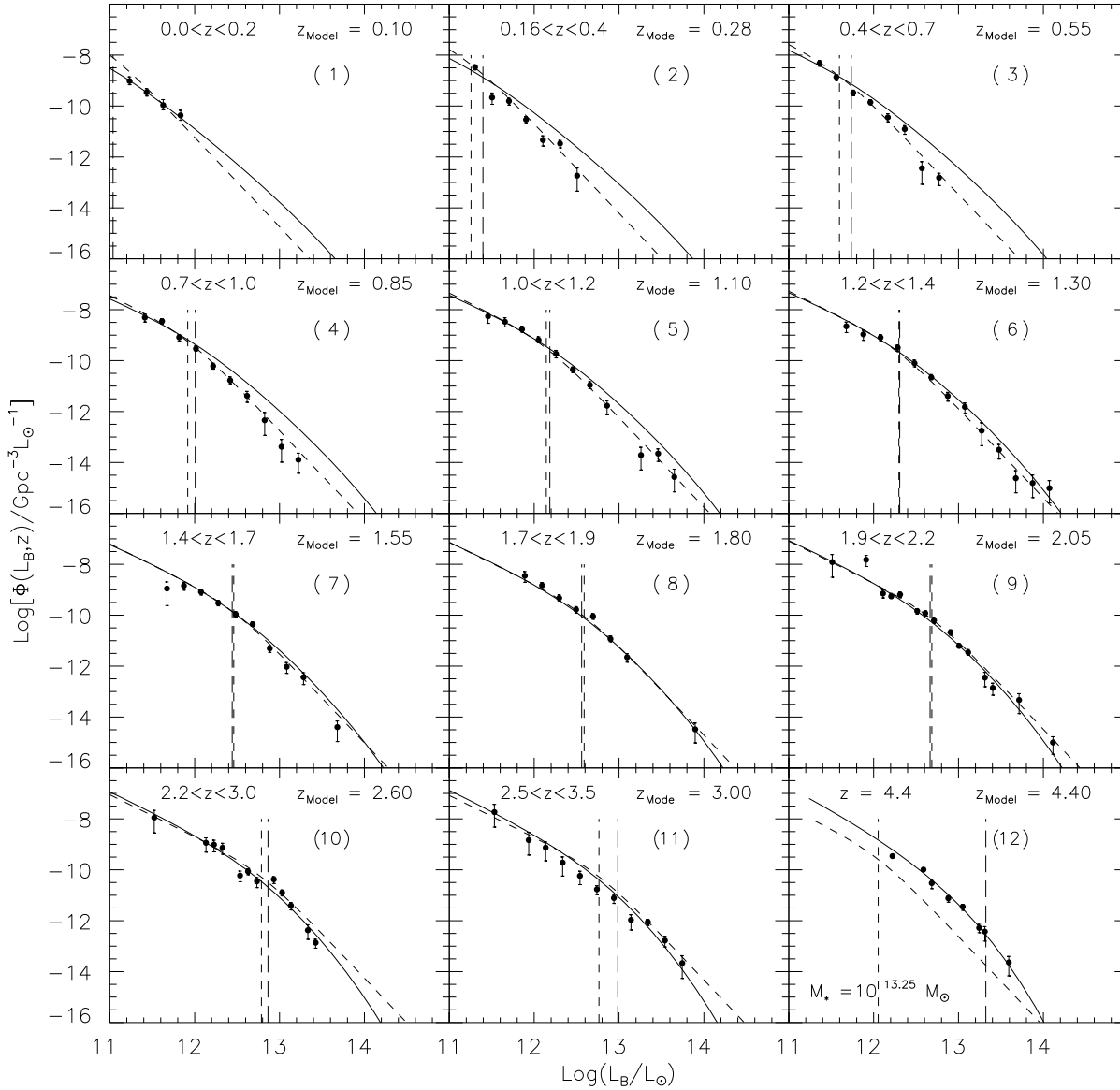


**Figure 6.** Model luminosity functions (solid curve) plotted against the observed luminosity functions (filled circle) of quasars. The data for  $z \lesssim 4$  is from Pei (1995) and for  $z \approx 4.4$  is from Kennefick, Djorgovski & Carvalho (1995). The model parameters are  $\epsilon_0 = 6 \times 10^{-6}$ ,  $\mu = 2$ ,  $M_* = 10^{13.25} M_\odot$  and  $t_{qso} \sim 0.035 t_{dyn}$ . The short-dashed curves show the double power law fit of Pei (1995). The long-dashed vertical line is the model break luminosity corresponding to  $M_*$  and the short-dashed vertical line is the characteristic luminosity in the double power-law fit.

noting that  $\Phi(L, z) \propto dV^{-1} dL^{-2}$  and  $L \propto d_L^2$ , where  $dV$  is the volume element and  $d_L$  is the luminosity distance (e.g. Hosokawa 2002). The double power-law is given as

$$\Phi_{obs}(L_B, z) = \frac{\Phi_*/L_z}{(L_B/L_z)^{\beta_l} + (L_B/L_z)^{\beta_h}}, \quad (23)$$

where  $\log(\Phi_*/\text{Gpc}^{-3}) = 2.95 \pm 0.15$ ,  $\beta_l = 1.64 \pm 0.18$  and  $\beta_h = 3.52 \pm 0.11$ . The characteristic luminosity  $L_z$  has a

Gaussian form

$$L_z = L_* (1+z)^{-(1+\alpha)} \exp\left[-\frac{(z-z_*)^2}{2\sigma_*^2}\right], \quad (24)$$

where  $\log(L_*/L_\odot) = 13.03 \pm 0.10$ ,  $z_* = 2.75 \pm 0.05$ ,  $\alpha = -0.5$  and  $\sigma_* = 0.93 \pm 0.03$ . In figure 6, the vertical short-dashed line is the characteristic luminosity given by equation 24 and the vertical long-dashed line shows the break luminosity for

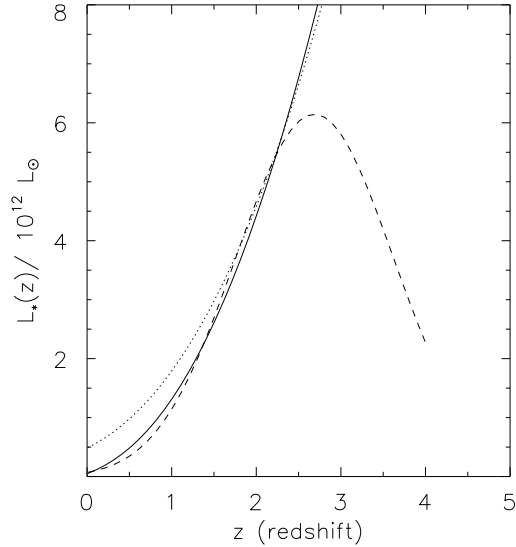


**Figure 7.** The evolution of break luminosity in our model (solid line) compared with the characteristic luminosity in the double power law luminosity function fit (dashed line). Also plotted is the break luminosity in a scenario where  $\epsilon = \epsilon_0$  is fixed (dotted line). The characteristic mass is  $M_* = 10^{13.25} M_\odot$ .

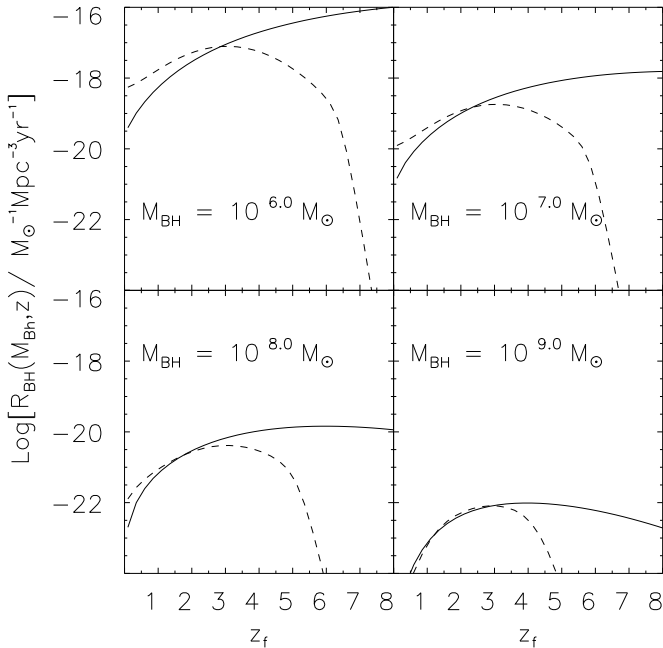


**Figure 8.** This figure shows the redshift evolution of formation rates of black holes with masses  $10^6, 10^7, 10^8$  and  $10^9 M_\odot$  respectively. The dashed lines are from equation 25 and the solid line are from equation 18

our model, corresponding to  $M_* = 10^{13.25} M_\odot$  haloes. It can be seen from the figure that the model can systematically account for the observed data over a wide range of redshifts. At  $z < 1$ , where the break luminosity of the model is slightly greater than the empirically fitted characteristic luminosity, we find that the bright end is slightly over predicted.

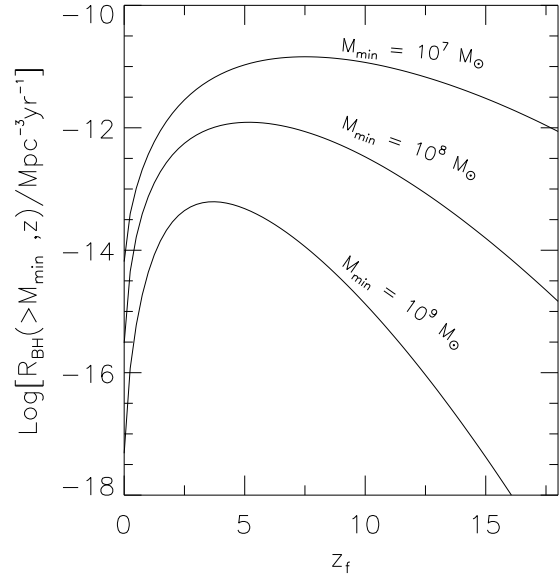


**Figure 9.** Cumulative formation rates of black holes with masses above  $10^7, 10^8$  and  $10^9 M_\odot$  respectively.

The characteristic luminosity and the break luminosity follow each other closely up to  $z \approx 2.5$ . This is especially clear in figure 7, where we additionally show (dotted curve) the break luminosity corresponding to  $M_*$  in a fixed black hole formation efficiency scenario.

It has been suggested in WL03 that rather than being an intrinsic feature of the quasars themselves, the break in the luminosity function is present only at low redshifts. Our model suggests otherwise. We find that the break in the luminosity function exists as a consequence of the characteristic mass and is present over a wide range of redshifts. Furthermore, the double power law in the form given above under-predicts the quasar luminosity function at  $z = 4.4$ . On the other hand, inserting the break luminosity given by our model into the double power law description of the data over-predicts the quasar luminosity function. A possible implication of this is that perhaps the black hole formation efficiency declines beyond  $z \sim 4$ .

The tuning of parameters for our model luminosity function is admittedly crude. Also, it can be seen from equations 16 and 20 that there exists a degeneracy between the parameters  $\epsilon_0$  and  $f_B$ . Higher values of  $\epsilon_0$  require systematically lower values of  $f_B$ . Nevertheless our fiducial numbers are in broad agreement with the values obtained by other investigations, and we emphasize once again that the model presented here only attempts to discern the broad trends of SMBH and quasar population evolution.

## 5 FORMATION RATES OF SMBH FROM THE OBSERVED LUMINOSITY FUNCTIONS

Due to their emission of gravitational waves, the merger rates of SMBHs will be detected directly by instruments such as the Laser Interferometer Space Antenna (LISA). In our model, SMBH merger/formation rates are given by equation



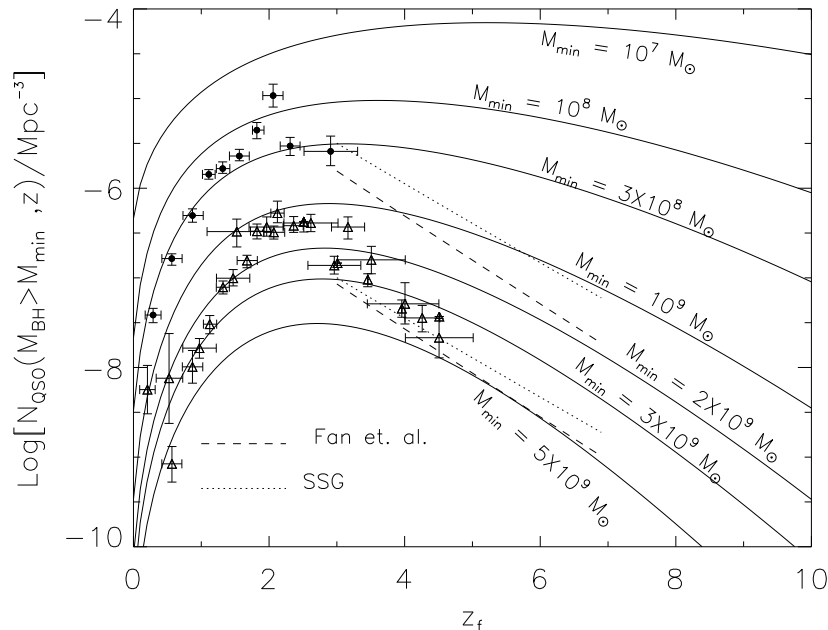


**Figure 10.** The space density evolution of quasars with minimum black hole mass  $M_{min}$  in the model, plotted against the observational data. Filled circles describe the observed space density evolution of quasars with absolute B-band magnitudes  $M_B < -24$  and open triangles describe the observed space density evolution of quasars with absolute B-band magnitudes  $M_B < -26$ . The data points are plotted as in Kauffmann & Haehnelt 2000 (see references therein). Also shown are the best fit to the high redshift data from Fan et al. (2001) (dashed lines) and Schmidt, Schneider & Gunn (1995) (dotted lines). The model parameters are same as in figure 6.

18. One can also use the double power-law fit to the luminosity function data to estimate these rates as a function of SMBH mass. These can be written as

$$R_{BH}^{obs}(M_{BH}, z) = \frac{1}{t_{qso}(z)} \times \Phi_{obs}[L_B(M_{BH}, z), z] \times \frac{dL_B}{dM_{BH}}(M_{BH}, z). \quad (25)$$

In figure 8 we plot SMBH formation rates for different masses using these two previous methods. The solid curves are computed from equation 18, i.e. our fiducial model, and the short-dashed curves are results from equation 25. The different masses considered are labelled in the figure. It can be seen that there is a significant discrepancy at high redshifts between the double-power law predictions and our model's. If, as discussed previously (section 4), the efficiency  $\epsilon$  declines beyond  $z \sim 4$ , a steeper decline in the SMBH formation rates at high redshifts would be obtained. This would of course bring the two estimates in better agreement. In other words, this would mean that our model only gives the maximum limiting value of SMBH formation rates at these redshifts.

In any case, it should be noted from the figure that the formation rates corresponding to  $10^6$  and  $10^7 M_\odot$  black holes are predicted to peak at very high redshifts ( $z \gtrsim 10$ ) and have greater values (at least a couple of orders of magnitude larger) than their more massive counterparts. Therefore, their detection (or lack of detection) by LISA would yield strong constraints on our understanding of the formation history of SMBH and their plausible minimum masses.

Figure 9 shows the cumulative formation rates of SMBH

computed by integrating equation 18 from a minimum black hole mass  $M_{min}$  to a tentative upper limit of  $\sim 10^{11} M_\odot$ . Note that the decline in the cumulative formation rates of SMBH towards low redshifts is much steeper as compared to the drop in the cumulative formation rates of haloes (figure 2).

The number density evolution of the quasars with SMBH masses above some minimum mass  $M_{min}$  can now be written as

$$N_{QSO}(M_{BH} > M_{min}, z) = \int_{M_{min}}^{M_{max}} dM_{BH} \times \{ t_{qso}(z) \times R_{BH}(M_{BH}, z) \}. \quad (26)$$

Figure 10 shows the the number density evolution of quasars with minimum black hole masses as labelled in the figure. Also plotted is the observed data for the space density evolution of quasars with minimum B-band magnitudes  $M_B < -24$  (filled circles) and  $M_B < -26$  (open triangles) up to a redshift of 10. As can be seen, the figure sketches a consistent picture with the original estimate of minimum quasar black hole masses of  $\sim 10^8 M_\odot$  by Soltan (1982).

## 6 THE MASS FUNCTION AND COSMOLOGICAL MASS DENSITY OF SMBHS

The formation rates of SMBHs can be used to compute their formation epoch distribution (see section 2.1). These can then be integrated over redshift to yield the SMBH mass

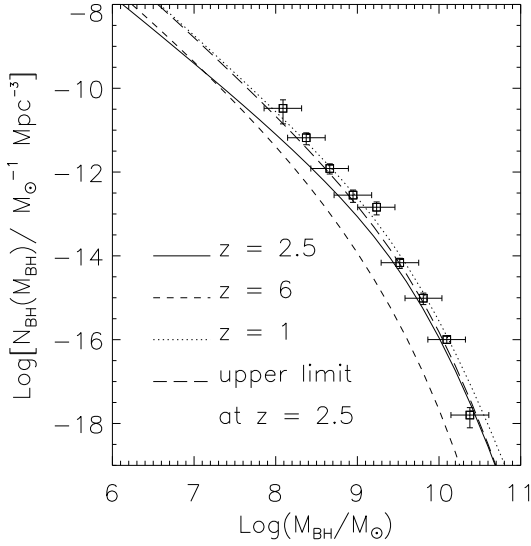


**Figure 11.** The mass function of SMBHs. Open squares show the local estimates given in Salucci et al. (1999). The limiting  $z = 2.5$  mass functions from our model have been plotted as solid line (using  $N_{BH}^A$ ) and long-dashed line (using  $N_{BH}^B$ ). We also show the upper limit mass function at  $z = 1$  (using  $N_{BH}^A$ ) and at  $z = 6$ , where both limiting mass functions ( $N_{BH}^A$  and  $N_{BH}^B$ ) are very similar.

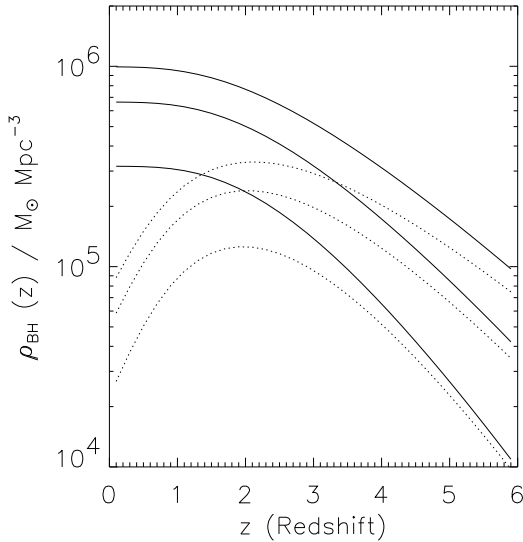


**Figure 12.** Comoving cosmological mass density of SMBHs by using the SMBH mass function  $N_{BH}^A$  (dotted lines) and  $N_{BH}^B$  (solid lines). Minimum SMBH masses  $M_{min}$  are (top to bottom)  $10^8$ ,  $3 \times 10^8$  and  $10^9 M_\odot$ . The two curves (solid and dotted) can be considered as (upper and lower) limits on densities for each  $M_{min}$ .

function. The formation epoch distribution of SMBHs can be written as

$$F_{BH}^A(M_{BH}, z_f \rightarrow z) = R_{BH}(M_{BH}, z_f) \times \frac{dt}{dz_f}(z_f) \quad (27)$$

$$\times P_{surv}[M_{halo}(M_{BH}, z_f), z_f \rightarrow z].$$

However, there are two problems with this equation. The first is that the survival probabilities of SMBHs are only crudely correlated to the halo survival probabilities: the declining merger rates of SMBH in haloes with mass above  $M_*$  suggest that the survival probability may be greater for SMBHs in these haloes. The second problem is more fundamental and lies in the fact that equation 16 is not only a function of halo mass but also of formation redshift. This can be understood in the following way: masses of SMBH for a given mass halo will be higher at high redshifts (this holds even if the formation efficiency is taken as constant such that  $\epsilon(z) = \epsilon_0$ ), so that when we compute the destruction probability  $P_{dest}$  of objects (note that  $P_{surv} = 1 - P_{dest}$ ), we authorise unrealistic situations where a halo with a higher mass black hole goes on to form a lower mass black hole. Hence we underestimate the survival probability. Equation 27, therefore, only gives a lower limit on the number counts of objects of different masses. An upper limit can be set by taking  $P_{surv} = 1$ . This amounts to computing mass functions by simply integrating the formation rates up to the redshift of observation. Such an approach has also been considered in Haehnelt & Rees (1993). Thus we write

$$F_{BH}^B(M_{BH}, z_f \rightarrow z) = R_{BH}(M_{BH}, z_f) \times \frac{dt}{dz_f}(z_f), \quad z_f \geq z. \quad (28)$$

We denote the corresponding SMBH mass functions as  $N_{BH}^A(M_{BH}, z)$  and  $N_{BH}^B(M_{BH}, z)$  respectively. These are computed as

$$N_{BH}^{A,B}(M_{BH}, z) = \int_{\infty}^z dz_f F_{BH}^{A,B}(M_{BH}, z_f \rightarrow z). \quad (29)$$

In figure 11 we plot the SMBH mass functions for several redshifts and compare them with the estimates of local SMBH mass function as given in Salucci et al. (1999). At redshifts greater than  $z \sim 3$  there appears to be no significant difference in the two limiting mass functions ( $N_{BH}^A$  and  $N_{BH}^B$ ). We can now write the comoving cosmological SMBH mass density as

$$\rho_{BH}^{A,B}(M > M_{min}, z) = \int_{M_{min}}^{\infty} dM_{BH} \{M_{BH} \times N_{BH}^{A,B}(M_{BH}, z)\} \quad (30)$$

Figure 12 shows the redshift evolution of cosmological mass density of the SMBH with minimum masses  $10^8$ ,  $3 \times 10^8$  and  $10^9 M_\odot$  (top to bottom) respectively. The solid lines are computed using  $N_{BH}^B$  and dotted lines are computed using  $N_{BH}^A$ . It can be seen that mass function  $N_{BH}^A$  gives an unrealistic decline in the mass density of SMBH which should increase monotonically. Once again, the reason is that the survival probability of the SMBHs are underestimated and thus the number counts are underestimated as well<sup>1</sup>.

<sup>1</sup> We point out that in a recent paper Bromley, Somerville & Fabian (2003) have found a similar non-monotonic evolution of SMBH mass density, computed by using the  $M - v_c$  relation combined with the Press-Schechter mass function.

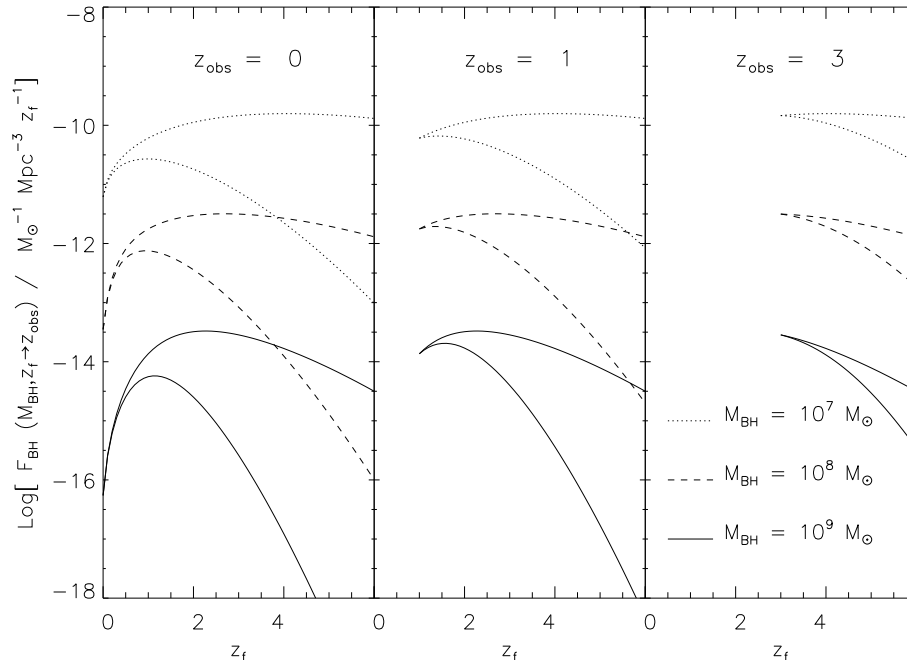


**Figure 13.** The contribution to the present day  $z = 0$  relic black holes from merger activity at higher redshifts. Different line-styles show results of the model for different black hole masses whose values are indicated in the figure. Each pair of curve in the same line-style indicates estimates using  $F_{BH}^A$  (lower curve) and  $F_{BH}^B$  (upper curve) as detailed in the text. It can be seen that at  $z = 0$ , a significant contribution comes from  $z \gtrsim 1$ .

The density computed using the mass function  $N_{BH}^B$  thus sets an upper limit to the density of SMBHs for the three different minimum masses.

In section 3 we have presented a scenario with a monotonically declining efficiency of black hole formation with decreasing redshift, with  $M_{BH} - v_c$  relation written as  $M_{BH} = \epsilon(z) v_c^5$ . However, the recent results of Shields et al. (2003) point towards a redshift independence of  $M_{BH} - \sigma$  relation (and therefore, by extension,  $M_{BH} - v_c$  relation). They find no discernible change in the relation up to redshift of  $z \approx 3$ . Thus they suggest that black holes are well formed by  $z \approx 3$ . In order to reconcile the redshift dependence of our model  $M_{BH} - v_c$  scaling with observed redshift independence of this relation, we present an argument based on the formation epoch distribution of the SMBH. In figure 13 we plot the formation epoch distribution of SMBH of different masses at different redshifts of observation  $z_{obs}$ . It is evident from the figure that most relic SMBH between redshifts  $z = 0$  and  $z = 1$  were formed at high redshifts  $z \gtrsim 1$ . As per our model, at redshifts  $z \gtrsim 1$ , the function  $\epsilon(z)$  does not vary significantly as  $z \approx 1$  is a characteristic redshift of decline for  $\epsilon(z)$ . Appreciable decline in  $\epsilon(z)$  occurs only at  $z \lesssim 1$ . Hence, our adopted redshift varying  $M_{BH} - v_c$  relation does not pose a problem with the observed redshift independence of the relation. Furthermore, it can be seen from figure 13 that using  $F_{BH}^B$  our model predicts that most relic SMBH between  $z = 0$  and  $z = 1$ , with masses above  $10^8 M_\odot$ , are formed between  $z \sim 2$  and 3. Whereas, using  $F_{BH}^A$  we predict that most SMBH were formed at  $z \sim 1$ .

## 7 ESTIMATES OF STAR FORMATION RATE AND NEUTRAL GAS DENSITY IN THE UNIVERSE

In our model, the declining black hole formation efficiency is attributed to a corresponding decline in the amount of cold gas mass available in galaxies. To estimate this cold gas mass, we take the fraction of cold gas  $f_{gas}(z)$  (which is different from the post merger fraction of cold gas available for accretion -  $f_{cold}$ ) in galaxies as proportional to  $\epsilon(z)$ , i.e.  $f_{gas}(z) \propto \epsilon(z)$ . For simplicity we assume that this fraction is independent of halo masses. We fix the constant of proportionality to match the amount of cold gas observed at high redshift in Damped-Ly- $\alpha$  systems. The cooling of gas in massive haloes may be ineffective (Benson et al. 2003) and therefore massive haloes may be deficient in cold gas. We, therefore, tentatively adopt an upper limit to the halo masses which are rich in cold gas as  $M_{max} \sim 10^{14} M_\odot$ , corresponding to cluster scales.

Using these simple prescriptions, we can write the mass of cold gas as  $M_{gas}(M, z) \propto \epsilon(z)M$ , where  $M$  is the halo mass. The comoving cosmological mass density of cold gas can then be written as

$$\rho_{gas}(z) = \int_{M_{min}}^{M_{max}} dM \{M_{gas}(M, z) \times N_{PS}(M, z)\}. \quad (31)$$

We take  $M_{min}$  as the minimum halo mass corresponding to the minimum halo circular velocity  $v_m$  for effectively retaining gas in the halo potential well (Somerville, Primack & Faber 2001). To simplify our computation we calculate  $M_{min}$  corresponding to  $v_{min}$  using equation 12 by setting the redshift of formation as the redshift of observation itself. This approach has been adopted

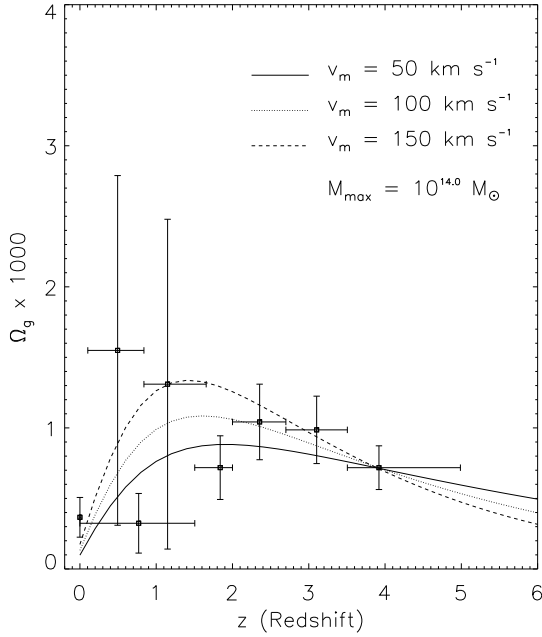


**Figure 14.** The evolution of comoving cosmological mass density of cold gas in galaxies as discussed in section 7. The data points are as given in Peroux et al. (2001), and the different line-styles correspond to estimates truncated at different low circular velocities indicated on the figure (see text for details).

previously, for example, in Robinson & Silk (2000), where they have discussed the error introduced by this simplification. Alternatively one can use the formation epoch distribution and convert it from masses to circular velocities and then integrate over all redshifts up to the redshifts of observation to get the circular velocity functions.

Dividing  $\rho_{gas}$  by the critical density  $\rho_c$  of matter in the universe we obtain  $\Omega_{gas}$ . This is plotted in figure 14 against the observations of Damped-Ly- $\alpha$  absorbers (Peroux et al. 2001). As previously mentioned, we have normalised  $\Omega_{gas}$  to the highest redshift data point in figure 14 which yields a constant of proportionality of the order of  $10^{-1}$  for the  $f_{gas}(z) - \epsilon(z)$  relation, with the exact value depending on the lower circular velocity cut-off used in the computation of  $\Omega_{gas}$ .

Further, the star formation rates can be estimated by adopting an SFR recipe as (e.g. Somerville & Primack 1999)

$$\dot{M}_* = \epsilon_* \frac{M_{gas}}{t_*}, \quad (32)$$

where  $\epsilon_*$  is the efficiency of star formation and  $M_{gas}$  is the cold gas mass available for star formation as described above. We can thus write the SFR density in the universe as

$$\rho_{SFR}(z) = \int_{M_{min}}^{M_{max}} dM \dot{M}_* \times N_{PS}(M, z). \quad (33)$$

Retaining the same normalisation as for the cold gas density, we choose  $t_* = 10^8$  years and an efficiency of 5 percent i.e.  $\epsilon_* = 0.05$ .  $M_{min}$  and  $M_{max}$  are as discussed for

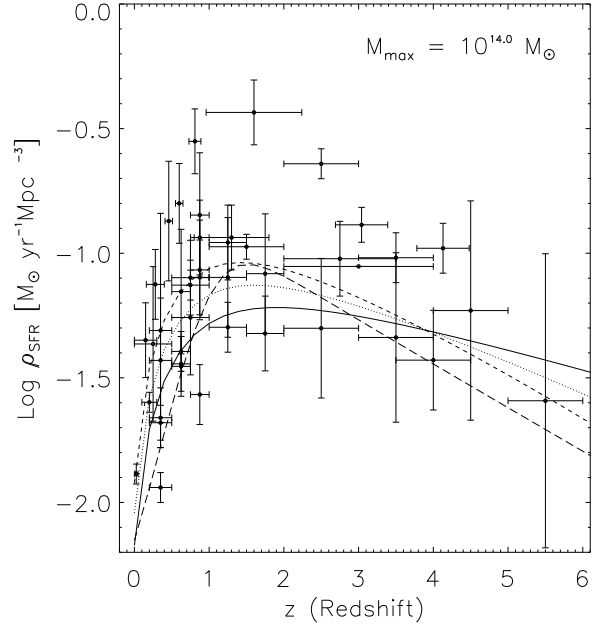


**Figure 15.** The evolution of SFR density in the universe. The different curves are results of the model with different minimum circular velocities using the same line-style code as in figure 14. The long-dashed curve is from the empirical SFR density evolution given in Madau & Pozzetti (2000). The data points with error bars are as compiled in Ascibar et al. (2002).

the case of cold gas density. Figure 15 shows the evolution of the SFR density in the universe.

It can be seen from the figure that our crude estimates for the cold gas density and the SFR density are broadly consistent with the data. This supports our assumption that there exists a correlation between the declining cold gas mass with redshift and the declining efficiency of black hole formation with redshift.

## 8 SIMPLE ESTIMATES OF THE QUASAR AND THE STAR FORMATION LUMINOSITY DENSITY IN THE UNIVERSE

Extending the analysis of SFR density and cold gas density in the universe, we now compute the relative contribution to the ionising background arising from the star formation rates and quasars. In the previous section we computed star formation rates by assuming a direct proportionality between the fraction of cold gas in galaxies and the efficiency of black hole formation. In a more realistic scenario, the cold gas content in galaxies builds up gradually, and is controlled primarily by two competing processes. The first process is that of gas condensation, whereby the gas loses energy over a cooling time scale and falls into the central baryonic core over a dynamical infall time-scale to form stars. The second process involves the expulsion of a fraction of this gas from the galaxy as a result of feedback from supernovae and AGNs. It seems reasonable, therefore, to suppose that the gas content in galaxies evolves dynamically, peaking at some epoch and declining afterwards.

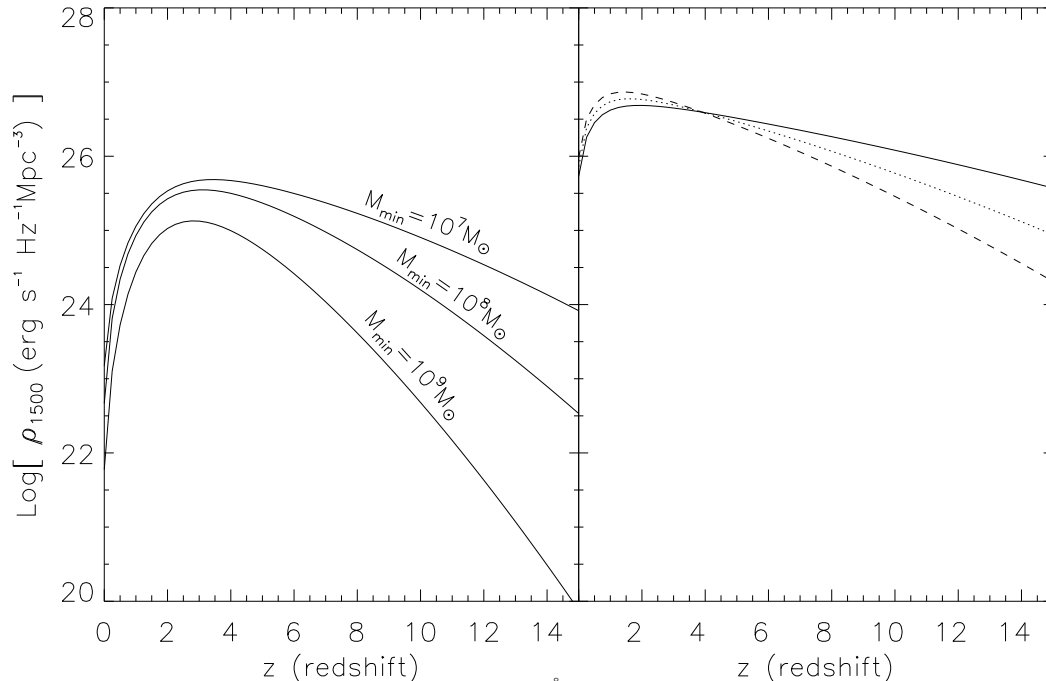


**Figure 16.** *Left panel:* The evolution of luminosity density (in 1500 Å) for quasars with minimum black hole masses  $M_{min} = 10^7$ ,  $10^8$  and  $10^9 M_{\odot}$  respectively. *Right panel:* The evolution of luminosity density (in 1500 Å) estimated from the star formation rates in the universe (see text for details). The line-styles are same as in figure 14.

However, in our model the black hole formation efficiency does not peak at high redshifts but reaches a maximum saturating value. Nevertheless, in view of the consistent results for the evolution of  $\Omega_{gas}$  and  $\rho_{SFR}(z)$ , we bypass the exact evolution history of  $\epsilon(z)$  and  $f_{gas}(z)$  by assuming their parallel evolution. This way we compute the maximal evolution of the luminosity densities for star formation rates and the quasars by extrapolating the model  $\epsilon(z)$  to high redshifts. It is possible that at high redshifts, the evolution of star formation rates as well as the black hole formation rates are driven predominantly by a rapid gravitational growth of structure (Di Matteo et al. 2003). Therefore, at these redshifts the exact evolution of  $\epsilon(z)$  and  $f_{gas}(z)$  is perhaps not so important.

Now the ultraviolet luminosity arising from star formation can be written as (Madau, Pozzetti & Dickinson 1998)

$$L_{UV} = C \times (\text{SFR} / M_{\odot} \text{yr}^{-1}) \text{ erg s}^{-1} \text{ Hz}^{-1}. \quad (34)$$

At 1500 Å, just longward of the hydrogen Lyman limit (e.g. HNR98), the value of  $C$  for a Salpeter IMF is given as  $C \approx 8 \times 10^{27}$ . Thus the ultraviolet star formation luminosity density is written as

$$\rho_{1500} = C \times \rho_{SFR}. \quad (35)$$

For quasars with a minimum black hole mass as  $M_{min}$ , the luminosity density in  $B$ -band can be written as

$$\rho_{4400}(z) = \int_{M_{min}}^{\infty} dM_{BH} \times \left[ \frac{L_B(M_{BH})}{\nu_B} \times t_{qso}(z) \times R_{BH}(M_{BH}, z) \right]. \quad (36)$$

Here,  $t_{qso}(z) \times R_{BH}(M_{BH}, z)$  is the number of active quasars with black hole mass  $M_{BH}$  existing at redshift  $z$ .

To convert the  $B$ -band luminosity into luminosity at 1500 Å, we adopt a power law spectral energy distribution scaling as  $L_{\nu} \propto \nu^{-\alpha}$  (Pei 1995), where  $\alpha = 0.5$  and  $L_{\nu}$  for a given band is simply  $L_{band} / \nu_{band}$ . In figure 16, we plot the evolution of luminosity densities due to star formation rates and quasars. These luminosity densities have also been estimated previously, for example, in Boyle & Terlevich (1998). For minimum black hole masses in the range  $10^7$  to  $10^9$ , we find that the drop in the quasar luminosity density towards low redshifts is steeper than computed in Boyle & Terlevich (1998). For minimum quasar black hole masses of  $10^8 M_{\odot}$  the curves in fig 16 suggest that at high redshifts, the ionising background is predominantly of stellar origin. It comes out from our calculations that quasar dominated ionising photon background is plausible if the minimum quasar black hole masses are  $\lesssim 10^7 M_{\odot}$  and the minimum circular velocities for haloes to effectively retain gas are fairly high ( $\sim 150 \text{ km s}^{-1}$ ). However, in light of the simplicity of the model used and the uncertainties involved in each of the estimates, these results should only be considered as indicative.

## 9 DISCUSSION AND CONCLUSIONS

We have presented an empirically motivated model for accretion dominated self-regulated growth of super massive black holes in galaxies and investigated their implications for the evolution of the quasar population in the universe. The model looks into the core aspects of quasar population such as the space density evolution of quasars, the evolution of the quasar characteristic luminosity, plausible minimum masses of quasars, the mass function of the super massive

black holes and the formation epoch distribution of these black holes.

The model suggests that the characteristic luminosity in the quasar luminosity functions arises primarily as a consequence of a characteristic mass-scale above which there is a systematic deviation of the black hole merging rates from the halo merger rates. Up to this mass-scale, the black hole merging appears to be closely following the merging of corresponding dark matter haloes. This anomalous behaviour is probably a consequence of rarer galaxy merging in massive haloes. Galaxies in massive haloes tend to retain their properties rather than quickly sink to the centre through dynamical friction. The extent of this effect might depend on the local environment of the merging galaxies. It is possible, for example, that galactic merging in massive haloes is efficient for high sigma peaks only. We have mimicked such a behaviour by introducing a simple phenomenological decline in the black hole formation rate through a function  $F_{\mu}(M)$  with a power law drop at the halo high mass end. When combined with a declining efficiency of black hole formation with redshift which we attribute to a decrease in the cold gas mass available, the model can reproduce the quasar luminosity function for a wide range of redshifts. Furthermore, we have shown that this declining black hole formation efficiency gives a better comparison of the model break luminosity evolution with the evolution of characteristic luminosity used in the empirical double power-law fit to the data.

On the lines of WL03, we have modelled time-scales for quasars proportional to the local dynamical time of the newly forming baryonic core, which in turn is proportional to the halo dynamical time. We found that the local dynamical time gives a better comparison with low redshift observations than the Salpeter time-scale. Furthermore, the adopted redshift varying time-scale allows a natural translation of the black hole formation rate density into number density of quasars, consistent with the the observed data.

Calculation of the number density evolution of quasars in our model also led us to infer plausible minimum masses of optical quasars on the order of  $\sim 10^8 M_{\odot}$ , consistent with the estimates of Soltan (1982) who computed minimum masses assuming a radiative efficiency of optical quasars  $\epsilon_{rad} = 0.1$ . Additionally, our model suggests a less steep decline of quasar number density at high redshifts than is generally assumed.

We also calculated the evolution of the comoving density of black holes with masses above  $10^8 M_{\odot}$  and  $3 \times 10^8$  and  $10^9 M_{\odot}$ . The possible reasons for anomalous non-monotonic evolution of  $\rho_{BH}$  inferred from the black hole mass function  $N_{BH}^A$  have been discussed. We find that for minimum black hole masses of  $10^9 M_{\odot}$  a density of at least  $\rho_{BH} \sim 10^5 M_{\odot} \text{Mpc}^{-3}$  has assembled by redshift of 2. The absolute upper limit for minimum SMBH masses of  $10^8 M_{\odot}$  is  $\rho_{BH} \sim 10^6 M_{\odot} \text{Mpc}^{-3}$ . These estimates are consistent with the estimates of local black hole density (Chokshi & Turner 1992; Salucci et al. 1999; Yu & Tremaine 2002). Our model suggests that a significant fraction of SMBH mass density was already in place by  $z \sim 2$  to 3. Interestingly, these estimates are also consistent with the recent results of Di Matteo et al. (2003). Moreover, the model SMBH mass functions at  $z \lesssim 2.5$  are consistent with the local mass function of SMBH derived in Salucci et al. (1999).

Finally, the predicted ionising background at high redshift appears to be predominantly of stellar origin. We find that a quasar dominated ionising background would need a lower limit of minimum SMBH masses along with a higher value of minimum circular velocities of haloes to effectively retain gas in them. Obscured low mass AGNs could thus raise the prospects of a quasar dominated ionising background. However, it is also possible that low mass AGNs have relatively low radiative efficiencies (e.g. Yu & Tremaine 2002) and thus may not be able to contribute effectively to the ionising background.

## ACKNOWLEDGEMENTS

A. M. wishes to thank Sugata Kaviraj, Ranty Islam, Claus Beisbart and Steve Rawlings for their help during the course of this work. Also, many thanks to Jeremy Blaizot for discussions, suggestions and his optimism about the present work. A. M. gratefully acknowledges the support from the Eddie Dinshaw foundation at Balliol College, Oxford. The research of J. E. G. D. at Oxford was supported by a major grant of the Leverhulme foundation.

## REFERENCES

- Ascasibar Y., Yepes G., Gottlober S., Muller V. 2002, *A&A*, 387, 396  
 Efstathiou G., Bond J. R., White S. D. M., 1992, *MNRAS*, 258, 1p  
 Benson A. J., Bower R. G., Frenk C. S., Lacey C. G., Baugh C. M., Cole S., preprint (astro-ph/0302450)  
 Binney J., Tremaine S., *Galactic Dynamics*, Princeton University Press, 1987  
 Bond J. R., Cole S., Efstathiou G., Kaiser N. 1991, *ApJ*, 379, 440  
 Bower R. J. 1991, *MNRAS*, 248, 332  
 Boyle B. J., Terlevich R. J. 1998, *MNRAS*, 293, 49  
 Boyle B. J., T. Shanks, S. M. Croom, R. J. Smith, L. Miller, N. Loaring, and C. Heymans, 2000, *MNRAS*, 317, 1014  
 Bromley J. M., Somerville R. S., Fabian A. C., preprint (astro-ph/0311008)  
 Bryan G., Norman M. L., 1998, *ApJ*, 495, 80B  
 Burkert A., Silk J., 2001, *ApJ*, 151, 154  
 Cavaliere A., Vittorini V., 2000, *ApJ*, 543, 599  
 Chokshi A., Turner E. L., 1992, *MNRAS*, 259, 421  
 Di Matteo T., Croft R. A. C., Springel V., Hernquist L., 2003, *ApJ*, 593, 56  
 Fan et al., 2001, *Astron. J.*, 121, 54  
 Ferrarese L., Merritt D., 2000, *ApJ*, 539, 9  
 Ferrarese L., 2002, *ApJ*, 578, 90  
 Gebhardt K. et al., 2000, *ApJ*, 539, 13  
 Haehnelt, M., Rees, M., 1993, *MNRAS*, 263, 168  
 Haehnelt, M., Natarajan, P., Rees, M., 1998, *MNRAS*, 300, 817 (HNR)  
 Haiman, Z., Ciotti L., Ostriker J. P., preprint (astro-ph/0304129)  
 Hatziminaoglou, E., Mathez, G., Solanes, J. M., Manrique, A., Sole, E. S., 2003, *MNRAS*, 343, 692  
 Hosokawa T., 2002, *ApJ*, 576, 75  
 Kauffmann G., Haehnelt M., 2000, *MNRAS*, 311, 576

Kennefick, J. D., Djorgovski, S. G., de Carvalho, R. R., 1995, *Astron. J.*, 110, 2553  
Kitayama T., Suto Y., 1996, *MNRAS*, 230, 638  
Lacey C., Cole S., 1993, *MNRAS*, 262, 627  
Lacey C., Cole S., 1994, *MNRAS*, 271, 676  
Madau P., Pozzetti L., Dickinson M 1998, *ApJ*, 498, 106  
Madau P., Pozzetti L., 2000, *MNRAS*, 312, 9  
Navarro, J. F., Frenk, C. S., White, S. D. M., 1997, *ApJ*, 490, 493  
Pei Y. C., 1995, *ApJ*, 438, 623  
Proulx C., McMahon R. G., Storr-Lombardi L. J., Irwin M. J. preprint (astro-ph/0107045)  
Robinson J., Silk J., 2000, *ApJ*, 539, 89  
Salucci P., Szuszkiewicz E., Monaco P., Danese L. 1999 *PASJ*, 637, 644  
Sasaki S., 1994 *PASJ*, 46, 427  
Schmidt M., Schneider D. P., Gunn J. E., 1995, *Astron. J.*, 110, 68  
Shaver P. A., Wall J. V., Kellermann K. I., Jackson C. A., Hawkins M. R. S., 1996, *Nature*, 384, 439  
Shields G. A., Gebhardt K., Salviander S., Wills, B. J., Xie B., Brotherton M. S., Yuan J., Dietrich M., 2003, *ApJ*, 583, 124  
Silk J., Bouwens, R., 2001 *New Astron. Rev.*, 45, 337  
Silk J., Rees M. J., 1998, *A&A*, 331, L1  
Soltan A., 1982, *MNRAS*, , 115S  
Somerville R. S., Primack J. R., 1999, *MNRAS*, 310, 1087  
Somerville R. S., Primack J. R., Faber S. M., 2001, *MNRAS*, 320, 504S  
Warren S. J., Hewett P. C., Osmer P. S., 1994, *ApJ*, 421, 412  
Wyithe J. S. B., Loeb A., 2003, *ApJ*, 595, 614  
Yu Q., Tremaine S., 2002, *MNRAS*, 335, 965

## APPENDIX A: A NOTE ON THE HALO MAJOR MERGER RATES

The halo major merger rates derived in section (2.1) are based on the approach of Kitayama & Suto (1996) whereby the major mergers are characterised as merger events in which an object at least doubles its mass. As pointed out in section 2, in this definition of major merger events, there is always a chance that the main progenitor has more than half the mass of the final halo, even though it is not supposed to. We discuss here how one can systematically account for this possibility and compute corrected major merger rates where no progenitor has more than half the mass.

Consider a merger event in which an object of mass  $M$  is formed from a progenitor of mass  $M_1$  ( $M_1 < M/2$ ). The mass accreted by this progenitor is  $M - M_1 = \Delta M$  ( $\Delta M > M/2$ ). This mass  $\Delta M$  can come either as a combination of formed smaller mass objects  $m_i$  such that  $\sum_i m_i = \Delta M$  or as a single formed object of mass  $\Delta M$ . In order to distribute the mass  $\Delta M$  (variance denoted as  $S_\Delta$ ) into smaller mass objects of mass  $m$  (variance denoted as  $S_m$ ) we use the Press-Schechter mass function (at time  $t$  corresponding to  $\omega \approx \omega_1 \approx \omega_2$ ). In the excursion set picture of Bond et al. (1991), the random walks of trajectories  $\delta(S_m)$  for the sub-clumps  $m$  now begin at  $S_m = S_\Delta$  instead of  $S_m = 0$ . This simply leads to an offset in the first passage distribution

function, which can be written as

$$f(S_m|S_\Delta)dS_m = \frac{1}{\sqrt{2\pi}} \frac{\omega}{(S_m - S_\Delta)^{3/2}} \exp\left[-\frac{\omega^2}{2(S_m - S_\Delta)}\right] dS_m. \quad (\text{A1})$$

The probability that none of the masses  $m_i$  is greater than  $M/2$  can be inferred from the ‘fraction’ of mass of  $\Delta M$  existing in objects below mass  $M/2$ . Thus

$$P_m[m < (M/2) | \Delta M] = \text{erf}\left[\frac{\omega}{\sqrt{2(S_h - S_\Delta)}}\right], \quad (\text{A2})$$

where  $S_h = S(M/2)$ . Note that when  $S_\Delta \rightarrow S_h$  this probability is one, that is all the masses  $m_i$  are less than  $M/2$ , as expected. Hence the corrected major merger rate is given as

$$\begin{aligned} R_{MM}(M, t) &= N_{PS}(M, t) \int_{S_h}^{\infty} dS_1 \frac{dP_1}{dt} P_m \\ &= N_{PS}(M, t) \left[-\frac{d\omega}{dt}\right] I(M, t) \end{aligned} \quad (\text{A3})$$

where  $I(M, t)$  is given as

$$I(M, t) = \int_{S_h}^{\infty} dS_1 \frac{1}{\sqrt{2\pi}} \frac{1}{[S_1 - S(M)]^{3/2}} \text{erf}\left[\frac{\omega(t)}{\sqrt{2(S_h - S_\Delta)}}\right]. \quad (\text{A4})$$

Unlike the expression for merger rates given in KS96, we find that  $I(M, t)$  here is a function of time. For any given mass  $M$ , therefore, KS96’s expression becomes more accurate as redshift increases (or for large  $\omega$ ) as  $P_m \rightarrow 1$ . Unfortunately the full expression for  $I(M, t)$  is not easy to evaluate. The difference becomes more pronounced at low redshifts, even though for massive haloes ( $> 10^{12} M_\odot$  at  $z = 0$ ) the discrepancy is too weak to affect the results presented in this paper. Hence for the purpose of deriving quasar luminosity functions and other properties we have restricted ourselves to the ‘computationally easy’ expression of KS96.

An additional advantage of equation A1 is that it could be used in the merger trees to sub-divide the remaining mass after picking the main progenitor at an earlier time in a short time-step. If this time step is very small, then in most cases the remainder mass is small and can be treated as accreted. In other cases, we think it more satisfactory to distribute the remaining mass (other than the main progenitor) according to equation A1 rather than use the various other methods that have been proposed in the literature.